

The distribution and extent of lunar swirls

Brett W. Denevi^{a,*}, Mark S. Robinson^b, Aaron K. Boyd^b, David T. Blewett^a, Rachel L. Klima^a

^a The Johns Hopkins University Applied Physics Laboratory, 11100 Johns Hopkins Road, Laurel, MD 20723, USA

^b School of Earth and Space Exploration, Arizona State University, Tempe, AZ 85287, USA



ARTICLE INFO

Article history:

Received 1 July 2015

Revised 12 November 2015

Accepted 12 January 2016

Available online 21 January 2016

Keywords:

Moon

Moon surface

Solar wind

Regoliths

ABSTRACT

The mysterious high-reflectance loops and ribbons known as swirls are not uncommon on the Moon, but are apparently unique to this body. We mapped their distribution and extent using ultraviolet-visible images from the Lunar Reconnaissance Orbiter Camera. We find two main geographic groupings of swirls (South Pole–Aitken Basin and Marginis–King) and a host of smaller features including swirls near craters Abel, Crozier, Dewar, and Dufay X. All mapped swirls are associated with magnetic anomalies and swirls have magnetic field strengths shifted to higher values than their background, though there is not a 1:1 correspondence between the locations of swirls and magnetic anomalies. Swirls are also found in regions with iron abundances shifted to higher-than-background values, which could indicate that their formation is inhibited by low iron content. The most distinguishing characteristic of swirls is a low 321/415 nm ratio coupled with moderate to high reflectance, and swirls generally have high optical maturity (OMAT) parameter values, stronger 1-μm bands, and shallower normalized continuum slopes than their surroundings, consistent with a surface that has experienced less space weathering. However, some swirls cannot be discerned in OMAT or band-depth images. Areas with low 321/415 nm ratios but non-distinct visible–near-infrared properties could be related to the presence of fresh silicates or a glassy component that does not have a substantial abundance of embedded large submicroscopic iron grains (i.e., a difference in the agglutinate fraction of the soil). Swirl color properties vary with distance from Copernican and some Eratosthenian craters; their association with Eratosthenian craters suggests fresh material may be preserved longer in swirls than in non-swirl regions.

© 2016 Elsevier Inc. All rights reserved.

1. Introduction

Among the myriad of beautiful lunar landscapes, albedo markings known as “swirls” may be among the most intriguing and confounding. With boundaries that are sometimes diffuse, sometimes sharp, they meander across the surface with no apparent regard for topographic or geologic variations beneath, as if painted with a giant brush (Fig. 1). Reiner Gamma, the tadpole-shaped swirl extending over 100 km across Oceanus Procellarum (McCauley, 1967), may be the type example, and swirls at Mare Marginis, Firsov crater, Mare Ingenii, (Strom and Whitaker, 1969; Whitaker, 1969; El-Baz, 1972) and a host of others are known (see list in Blewett et al., 2011). These swirls range from large groupings of many complex loops and ribbons to a single isolated feature (Blewett et al., 2011); scales are typically in the tens of kilometers, and groupings of swirls can cover hundreds of kilometers.

Early work hypothesized that swirls could be volcanic deposits, such as from a felsic nuée ardente (McCauley, 1967), sublimes (Whitaker, 1969; El-Baz, 1972), or the products of chemical alteration from volcanic gases (El-Baz, 1972). However, two key sets of observations shaped subsequent formation theories. First, it was recognized that swirls are associated with crustal magnetic anomalies (Hood et al., 1979b; Hood and Schubert, 1980). Second, the spectral properties of swirls are similar to those of Copernican craters and ejecta, as first noted for Reiner Gamma (Hood et al., 1979b). This second point was repeatedly confirmed across the electromagnetic spectrum. From short to long wavelengths, the spectral properties of swirls are similar to those of fresh impact craters and ejecta and include: low far-UV reflectance values (Hendrix et al., 2015); steep UV slopes (Denevi et al., 2014); high visible–near-infrared reflectance and low 950/750 nm ratio values (Blewett et al., 2011; Kramer et al., 2011a); shallower visible–near-infrared continuum slopes and stronger mafic (1 and 2 μm) absorptions (e.g., Bell and Hawke, 1981; Kramer et al., 2011b); and thermal-infrared Christiansen Feature wavelengths shifted to short values (Glotch et al., 2015).

* Corresponding author.

E-mail address: brett.denevi@jhuapl.edu (B.W. Denevi).

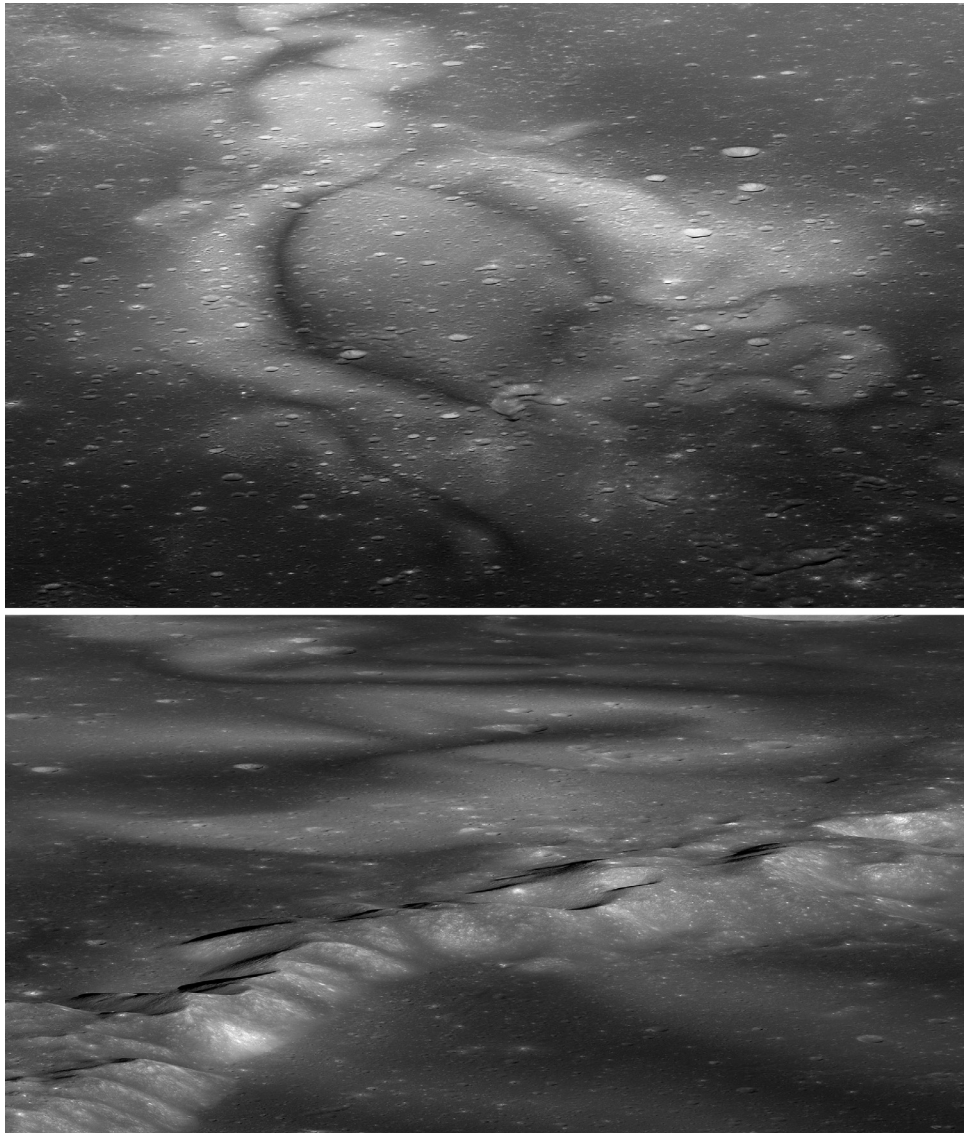


Fig. 1. Oblique views of swirls from the Lunar Reconnaissance Orbiter Camera Narrow Angle Camera (NAC). Top: Reiner Gamma seen from the west looking east, NAC image M1127569280L,R. Bottom: Mare Ingenii swirl seen from the east looking west, NAC images M191830503L,R. Both images are ~60 km wide at center.

These spectral properties are consistent with materials that have experienced less space weathering than typical lunar soils. Space weathering is the collection of physical (communition, vitrification, agglutination) and chemical (reduction of ferrous iron to iron metal) changes that result from micrometeoroid bombardment and interactions with the solar wind (e.g., Hapke, 2001). Thus if the swirls are indeed immature (have experienced low degrees of space weathering), they must have either formed recently or have avoided the typical space weathering processes. These two scenarios lead to two formation models: swirls formed recently, due to cometary impacts (Schultz and Srnka, 1980; Bell and Hawke, 1987; Pinet et al., 2000; Starukhina and Shkuratov, 2004; Bruck Syal and Schultz, 2015) or swirls avoided the typical space weathering process, due to magnetic shielding from the solar wind (Hood and Schubert, 1980; Hood and Williams, 1989; Kramer et al., 2011b; Glotch et al., 2015).

In the comet impact model, the high-reflectance of swirls is due to recent scouring of the surface by large amounts of vapor generated by the extremely high-velocity nucleus impact, as well as scouring from impacting dust and ice particles from the in-

ner coma (Schultz and Srnka, 1980; Bruck Syal and Schultz, 2015). The scouring is proposed to expose fresh regolith or to result in the compaction of regolith (or both), and the turbulence of the gas flow over the surface produces the distinctive swirl shapes. The local magnetic anomalies in this case are thought to result from magnetization of hot material in a transient magnetic field created by compression of the comet's intrinsic magnetic field (Gold and Soter, 1976; Schultz and Srnka, 1980; Bruck Syal and Schultz, 2015) or charge separation between plasma and ejecta (Crawford and Schultz, 1999; Bruck Syal and Schultz, 2015). Swirls at Reiner Gamma and Mare Marginis have unusual photometric properties; they are more forward scattering than other high-reflectance deposits such as crater ejecta. The enhanced forward scattering is thought to indicate lower millimeter-scale roughness and greater compaction of the regolith (Schultz and Srnka, 1980; Pinet et al., 2000; Kreslavsky and Shkuratov, 2003; Kaysdash et al., 2009), which could be explained by the scouring from the comet impact. However, the thermophysical properties of the swirls are nearly identical to those of their surroundings, inconsistent with roughness or compaction differences (Glotch et al., 2015),

suggesting the photometric behavior may have another cause. Additionally, no swirls are found on Mercury, despite the higher influx of cometary impactors (Blewett et al., 2010).

The shielding model for swirl formation proposes that pre-existing crustal magnetic anomalies deflect the solar wind, reducing the rate of space weathering (sputtering and/or H implantation) in the high albedo regions of swirls (Hood et al., 1979a; Hood and Schubert, 1980; Hood and Williams, 1989). While the origin of magnetic anomalies is not critical to an understanding of the solar wind shielding model, it has been proposed that plasma clouds from large hypervelocity impacts converge and amplify preexisting ambient fields at basin antipodes; this coincides with seismic compression and high shock pressures at the antipode, leading to shock remanent magnetization (e.g., Hood and Williams, 1989; Hood and Huang, 1991; Mitchell et al., 2008; Hood et al., 2013). Whatever their origin, crustal magnetic anomalies have been shown to create mini-magnetospheres (Halekas et al., 2008; Wieser et al., 2010) and deflect solar wind protons at swirl sites (Lue et al., 2011), consistent with observations of shallower OH/H₂O absorptions at 2.8 μm for swirls (Kramer et al., 2011b; Pieters and Garrick-Bethell, 2015). The distinctive shapes of the swirls are interpreted to be due to the orientation of the local magnetic field lines, with high-reflectance regions corresponding to dominantly horizontal fields (Hemingway and Garrick-Bethell, 2012). If this model is correct, space weathering on the Moon must be dominated by the effects of the solar wind, as space weathering due to micrometeoroid bombardment would continue unimpeded. Additionally, it is unlikely that the magnetic shielding is perfectly efficient, raising the question as to why swirls do not eventually mature. **Lunar space weathering results in optical maturation in the visible and near-infrared range on the scale of hundreds of millions of years** (e.g., Grier et al., 2001), and observations of deflected proton flux suggest a shielding efficiency of 10–50% (Lue et al., 2011), though orbital measurements of magnetic field strength from relatively high altitudes (>30 km) do not fully characterize conditions at the surface. **One possible explanation is that swirls are periodically “refreshed” by outside crater ejecta** (Hood et al., 1979a, 1979b, 2001; Blewett et al., 2011); another is that swirls do mature to some extent, but reach a steady-state that is distinct from that of typical mature regolith (Hemingway et al., 2015). The idea that swirls have reached some level of maturity is consistent with the observation that the ejecta of fresh craters within swirls is higher in reflectance with stronger band depths than average swirl regolith (Kramer et al., 2011a).

In addition to the comet impact and solar wind shielding hypotheses, a third scenario posits that the high reflectance of swirls is not due to either the recent exposure of fresh material or reduced space weathering. Instead, the magnetic anomalies result in the sorting of soil grains (Garrick-Bethell et al., 2011; Pieters and Garrick-Bethell, 2015). One variation suggests that electrostatically levitated dust grains are attracted or repelled by electric potentials created by the magnetic anomaly (Garrick-Bethell et al., 2011). The accumulation of this levitated and redeposited dust in swirls leads to a surface that is higher in reflectance because of its small particle size and because the finest fraction of lunar soils is preferentially enriched in a feldspathic component (Garrick-Bethell et al., 2011). The smallest size fraction of lunar soils has been shown to be highly mature (Pieters et al., 1993); to account for the spectral properties that are more consistent with swirl surfaces having experienced less space weathering, Garrick-Bethell et al. (2011) suggested that newly created dust may be transported to the swirls rather than mature dust, or that the optical path length is enhanced by the presence of finer materials, increasing local absorption bands. These last explanations are rather unsatisfying, but recent work has questioned whether mafic absorption bands in swirls actually are stronger than surrounding mature terrain

(Pieters et al., 2014), leading to a modified sorting model, wherein the mature soils are magnetically sorted due to their iron metal content (Pieters and Garrick-Bethell, 2015), as has been demonstrated in laboratory work where agglutinates can be magnetically removed from the bulk soil (Adams and McCord, 1973). The magnetic removal of low-reflectance agglutinates from swirl surfaces would be consistent with the swirls' overall high albedo.

Here we step back from the increasingly detailed views of lunar swirls to present a broad perspective enabled by images from the Lunar Reconnaissance Orbiter Camera (LROC) Wide Angle Camera (WAC) (Robinson et al., 2010). Initial work showed that the swirls have distinct ultraviolet characteristics that make them conspicuous in WAC color images (Denevi et al., 2014); we make use of these characteristics to produce a comprehensive map of swirls across the lunar surface. This map permits a global assessment of swirl characteristics such as maturity, spectral properties, composition, local magnetic field strength, and topographic variation. While discriminating between various models for lunar swirl formation may be unresolvable without additional data, new comprehensive knowledge of the distribution and characteristics of swirls can be used to further inform our knowledge of these inscrutable features and provide a basis for future studies.

2. Data and methods

A global color mosaic from the LROC WAC was used as the primary basis for our lunar swirl study. The LROC WAC is a push-frame camera that acquires images through seven narrow-band filters with central wavelengths ranging from 321 through 689 nm (Robinson et al., 2010). Each month, the WAC obtains near-global coverage of the Moon; the color mosaic used here is the product of ~36 months of WAC observations, and the value at each pixel is the median of all observations for that geographic location after photometric normalization (Boyd et al., 2012). The mosaic is sampled at 76 pixels/degree (~400 m/pixel), which is the approximate native pixel scale of the UV filters (321, 360 nm) and an undersampling of the visible filters (415, 566, 605, 643, and 689 nm, native resolution ~100 m/pixel). An empirical WAC-derived photometric normalization to a standard lighting and viewing geometry (incidence, emission, and phase angles of 30°, 0°, and 30°) was employed (Boyd et al., 2012), using incidence and emission angles calculated with respect to local topography derived from the global lunar digital terrain model with a sampling scale of 100 m (GLD100; Scholten et al., 2012). Due to an increasing fraction of shadows and larger phase angles at high latitudes, we limit our study to ± 60° latitude.

Swirls were identified in a WAC color composite, where 415 nm reflectance was displayed in red, the 321/415 nm ratio was in green, and the 321/360 nm ratio was in blue (Fig. 2). This color combination highlights spectrally immature regions and allows for the confident detection of swirls (Denevi et al., 2014). In areas with FeO contents above ~5 wt%, immature regions have high 415 nm reflectance, and low UV/visible ratios due to the steep decrease in reflectance at wavelengths shorter than ~450 nm. This drop-off in reflectance at short wavelengths results from strong charge-transfer absorption bands centered below ~300 nm in silicates (e.g., Wells and Hapke, 1977); the slope shallows with the addition of nanophase iron that forms as a result of exposure to space weathering (Hendrix and Vilas, 2006; Hendrix et al., 2012; Denevi et al., 2014). In areas of lower FeO dominated by plagioclase, the drop-off in reflectance occurs at shorter wavelengths and is seen as a break in slope at 360 nm rather than at 415 nm (Denevi et al., 2014).

In addition to the WAC color composite, a 643-nm WAC normalized reflectance map was used to examine swirls initially identified based on their color properties. This map was sampled at

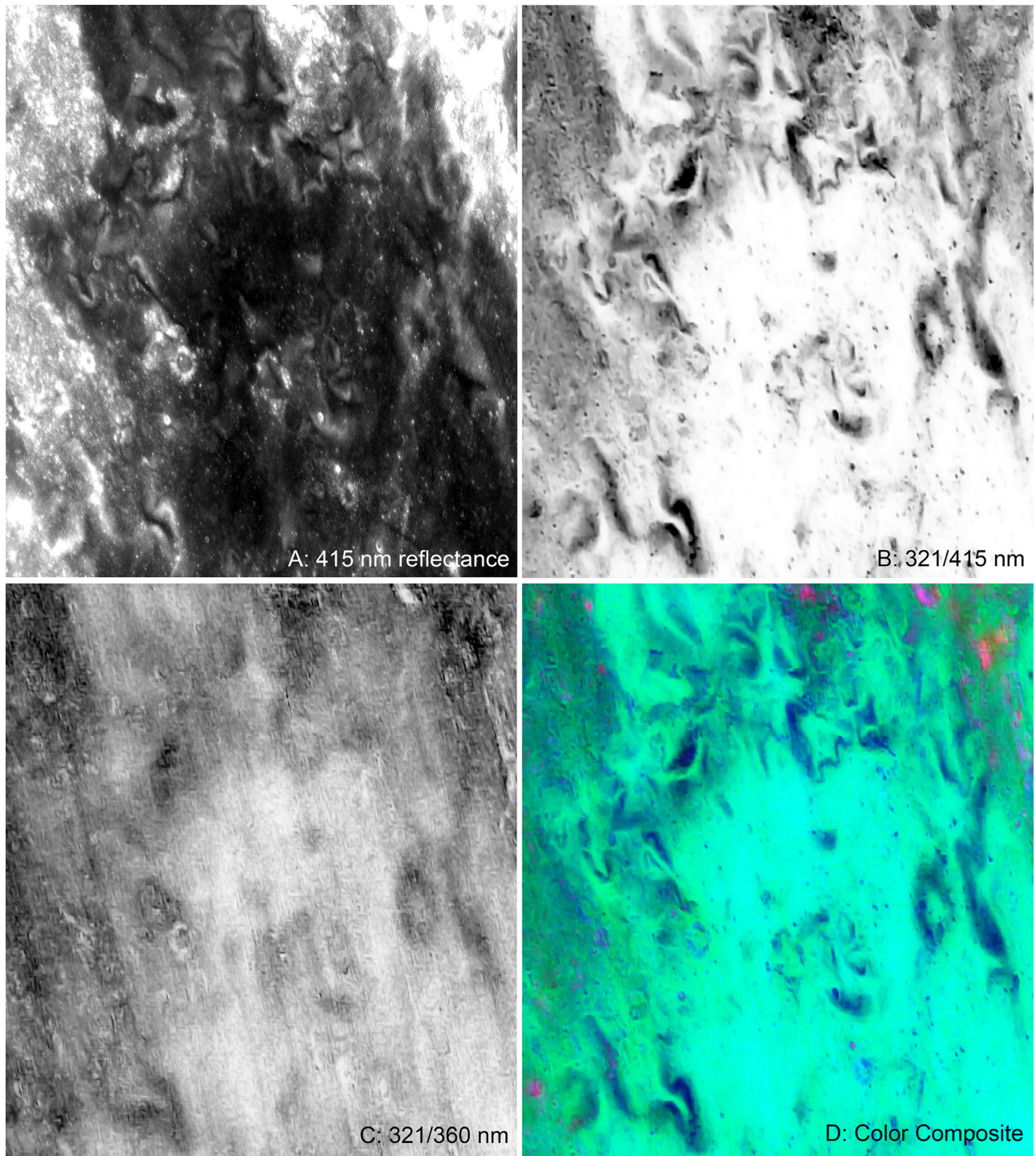


Fig. 2. Example components of the WAC color composite that was used to identify swirls for a portion of the Mare Marginis region. In this composite, the 415 nm reflectance (A) is displayed in red (swirls have relatively high reflectance), the 321/415 nm ratio (B) is shown in green (swirls have a low ratio value) and the 321/360 nm ratio is shown in blue (swirls have a low ratio value). The red, green, blue composite is shown in (D). Orthographic projection centered at 0°N, 30°E; scene centered at 13°N, 84°E, scene width is 120 km.

100 m/pixel, and compiled from images acquired with low incidence angles that highlight albedo differences. A complementary map, compiled from WAC images acquired with higher incidence angles was used to examine the swirls in the context of local topographic variations, which may have some residual effect on the reflectance maps at high latitudes where there are persistent shadows. After examining features in each of these three basemaps, the

margins of swirls were mapped at the full resolution of the WAC color mosaic (400 m/pixel). For diffuse features, the recorded swirl extent is necessarily approximate and was determined on the basis of the extent of the feature in the color composite image.

After the swirls were identified within $\pm 60^\circ$ latitude, they were characterized in terms of the local total magnetic field strength at 30-km altitude (Richmond and Hood, 2008), local slope

derived from the WAC stereogrammetric digital terrain model (the GLD100 from Scholten et al., 2012) over a 1-km baseline, spectral continuum slope and mafic band depth from Moon Mineralogy Mapper (M^3) spectra (Pieters et al., 2009; Boardman et al., 2011), Lunar Prospector Gamma-Ray Spectrometer (GRS) derived iron content (Lawrence et al., 2002), and Clementine optical maturity (Lucey et al., 2000). We have elected to use the GRS-derived FeO values rather than those derived from reflectance spectroscopy (e.g., Lucey et al., 1995), as previous work has noted that the spectral trends of the swirls do not follow those of typical lunar soils (Blewett et al., 2011; Hemingway et al., 2015). As the optical maturity (OMAT) parameter is calculated in a complementary manner to spectrally derived FeO (Lucey et al., 1995, 2000), we note that the OMAT values for swirls likely do not allow for a 1:1 comparison with the OMAT values of typical immature soils such as those exposed at fresh impact craters. For each individual mapped feature, mean values from each of these datasets were computed by averaging over the area of that feature. For most of the datasets, this meant averaging many pixels within each feature; for the Lunar Prospector derived measurements (magnetic field strength, FeO abundance), it was simply recording the local value if the feature in question was smaller than the map scale (15 km/pixel).

3. Results

The distribution of swirls as determined from LROC WAC images is shown in Fig. 3. The general distribution is consistent with most previously identified swirls (El-Baz, 1972; Schultz and Srnka, 1980; Hood, 1995; Blewett et al., 2011). Major differences include: (1) We find swirls within the South Pole–Aitken (SPA) basin to be much more extensive and continuous in our WAC-based map. (2) We find swirls in four additional locations: Abel, Crozier, Dewar, and Dufay X (described below).

3.1. South Pole–Aitken basin swirls

Mapping of the swirls in the SPA basin reveals them to be one essentially continuous geographic group that stretches over 50° in longitude and nearly 1000 km in extent from southwest to northeast (Fig. 4a). Swirls in this region were previously identified in what appeared to be several discrete groupings (Schultz and Srnka, 1980; Hood, 1995), such as those at Hopmann, Ingenii, and Northwest of Apollo as described by Blewett et al. (2011). The highest density of swirls not previously mapped is a large stretch between Birkeland and Leeuwenhoek craters to the east of Mare Ingenii in a region of highland terrain within SPA (Fig. 5). This area has over 80 individual swirls that are tightly clustered with complex loops and ribbons. They extend inside the rim of Birkeland crater and drape across the rough topography of the area (Fig. 5). Other large concentrations of swirls that are newly identified here are found to the far north and southwest of Mare Ingenii (Fig. 4).

In all, we identified over 400 individual features within the SPA swirl group. The mapped swirls extend to a latitude of 54° S. We suspect that there may be more swirls in this southern region, but did not extend our map further because differences in normalized reflectance due to topographic effects become more pronounced in the area, despite the fact that local photometric angles were computed using the GLD100 digital terrain model.

The swirls in SPA generally have moderately elevated 415 nm reflectance, and low 321/415 and 321/360 nm ratio values, so that they appear in shades of blue to pink or red in the WAC color composite (Fig. 5b), compared to the mature background with its high 321/415 nm ratio and low reflectance (green in the color composite). In many places, the color of fresh craters is distinct from that of the swirls; the difference lies largely in the higher 415 nm reflectance values of fresh craters (the red channel), which results

in fresh craters appearing more red or pink in this color scheme. Several relationships between swirls and small impact craters of differing states of maturity are noted. Fresh impact craters with a continuous, high-reflectance ejecta deposit (Copernican in age) appear to superpose any swirls in their immediate vicinity. Swirls can be discerned up to the edge of the fresh ejecta, but closer to the crater swirls cannot be distinguished from amongst the fresh crater ejecta in the color composite (Fig. 5b). In contrast, examples are found where the crater is morphologically fresh, but has no continuous high-reflectance ejecta deposit (Eratosthenian in age). In this case, swirls are observed nearly up to the rim of the crater, and their color properties are similar to those of the nearby Copernican impact crater (Fig. 5b).

3.2. Marginis–King swirls

The second major geographic grouping of swirls extends from Mare Marginis to the east of King crater, and includes the prominent swirls located by Firsov crater. This group is of comparable scale to the grouping in SPA, covering over 1000 km east-to-west and includes just over 400 individual features (Fig. 6). The large extent of the swirls in this region was originally recognized in Apollo 16 images (El-Baz, 1972) as the Alhazen to Abul Wafa swirl belt (Marginis–King has the benefit of more recognizable landmarks that better define the extent mapped here). As opposed to the SPA swirls, we find neither more individual swirls nor a broader distribution of the swirl group; our map is remarkably similar to that of Schultz and Srnka (1980).

Swirls in this region are found within rays of Giordano Bruno, King, and Goddard A craters (Fig. 6, 7). Superposition relationships with these rays cannot be clearly discerned. Swirls within the Giordano Bruno rays are far from the crater itself (generally > 500 km, though the closest feature is ~ 280 km distant) and have 643 nm reflectance values that are comparable to or higher than those of the rays (Fig. 7a), which are fairly diffuse and discontinuous at these distances. The same is seen for swirls near King and Goddard A, where the reflectance of swirls is also comparable to or slightly higher than the reflectance of the rays (Fig. 7b and c). Some swirls have been shown to have “dark lanes” – areas between high-reflectance swirls with reflectance values lower than nearby mature terrain (Coman et al., 2011; Garrick-Bethell et al., 2011; Glotch et al., 2015). The inter-swirl areas in Fig. 7 are comparable to the background terrain near the crater and higher than the background terrain further from the crater, and we find no definitive examples of dark lanes that cross any rays.

As with the example in SPA, swirls around the crater Goddard A have color properties similar to Copernican crater ejecta when close to the crater, and lower reflectance and lower UV ratio values further from the crater (Fig. 8a and b); the same relationship is seen with swirls at increasing distances from King crater (Fig. 8c and d).

3.3. Other swirls

In LROC WAC data, we find no major differences in the extent of swirls described by Blewett et al. (2011) at Airy, Moscoviente, Gerasimovich, and Reiner Gamma; at Rima Sirsalis we find several additional small swirls. WAC color images allowed for the identification of swirls at two of the prominent magnetic anomalies for which Blewett et al. found no associated features, Abel and Crozier (Fig. 9a–f). At both of these locations, diffuse albedo anomalies ~ 50 km across are observed (Fig. 9c and f); the low 321/415 nm ratios aid in discriminating the swirl features from other albedo features in each region (Fig. 9b and e). Each is a single, isolated feature similar to the simple swirl at Airy (Blewett et al., 2011).

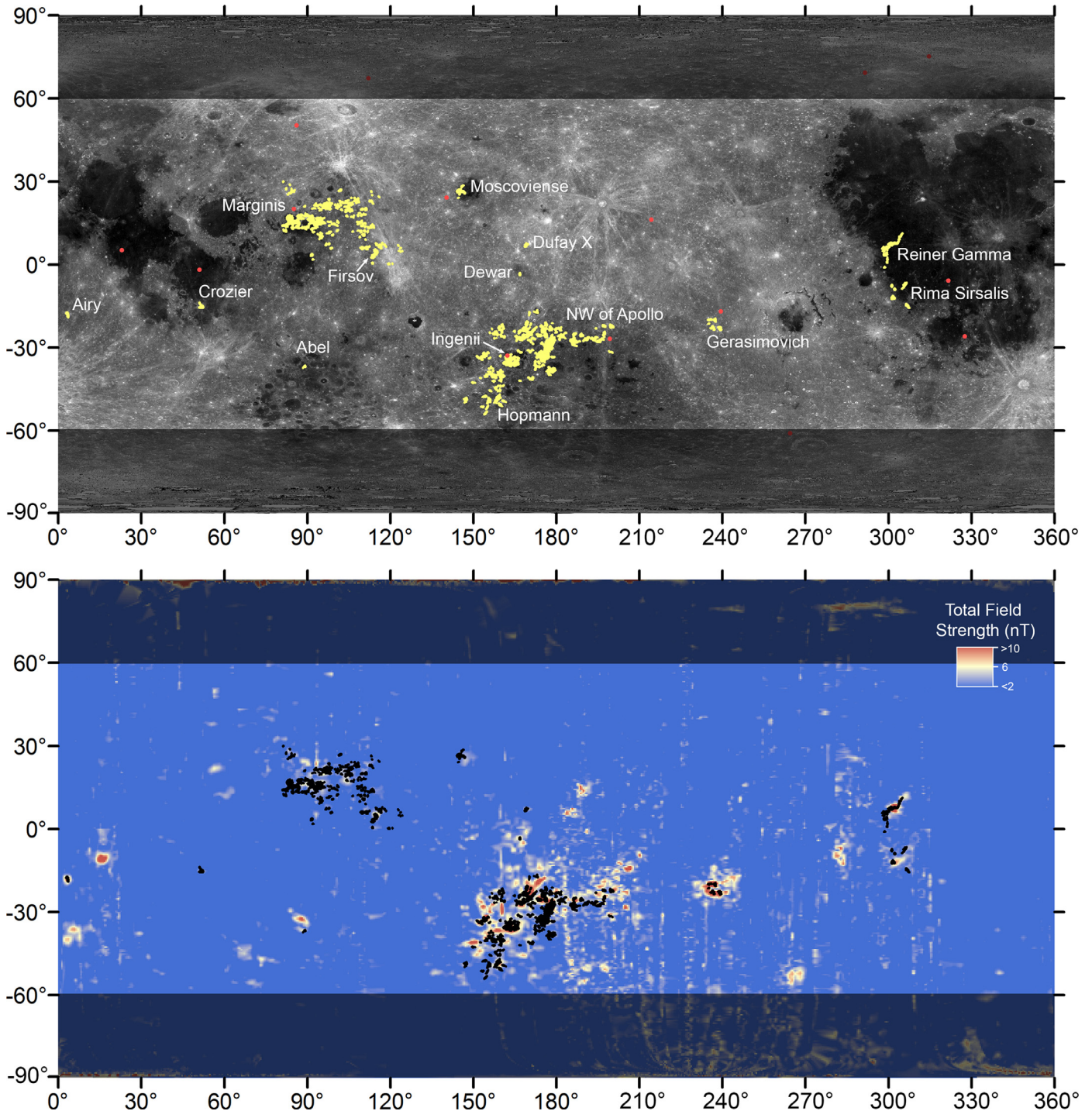


Fig. 3. LROC WAC-based map of lunar swirl locations. Top: swirls are shown in yellow on a WAC 643 nm reflectance map. Labels correspond to regions examined by Blewett et al. (2011), with the addition of Dufay X and Dewar. The locations of the antipodes of the youngest lunar basins (Nectaris–Orientale) (Wilhelms, 1987) are indicated with red dots. Bottom: swirls shown in black on a map of total magnetic field strength at 30-km from Lunar Prospector (Richmond and Hood, 2008). WAC color data used to identify swirls is most reliable within $\pm 60^\circ$ latitude; higher latitudes are shaded. Note that the outlines of swirls are shown in bold to make them more visible at this scale, thus features are slightly exaggerated in size. Lunar circumference is 10,917 km (width of map at equator).

Swirls are identified at two additional locations: Dewar (Fig. 9g–i), and Dufay X (Fig. 9j–l). The swirl at Dewar is similar to those at Abel and Crozier and consists of a single, isolated loop ~ 25 km in extent. The Dewar region is associated with a magnetic anomaly (Fig. 3), and has also been identified as a cryptomare deposit with elevated iron, titanium, and thorium concentrations (Lawrence et al., 2008). The swirl at crater Dufay X is ~ 50 km across, but is more complex than the Dewar feature, hav-

ing multiple smaller loops and bends. In addition to the swirl, a high-reflectance diffuse feature is observed to the east (Fig. 9l). This albedo anomaly does not have the characteristic swirl shapes, and is not mapped as such. However, it does have a strong UV absorption, with low 321/415 nm ratios (Fig. 9k). Another diffuse albedo anomaly of similar size was identified in association with the magnetic anomaly at Descartes (Richmond et al., 2003; Blewett, 2005).

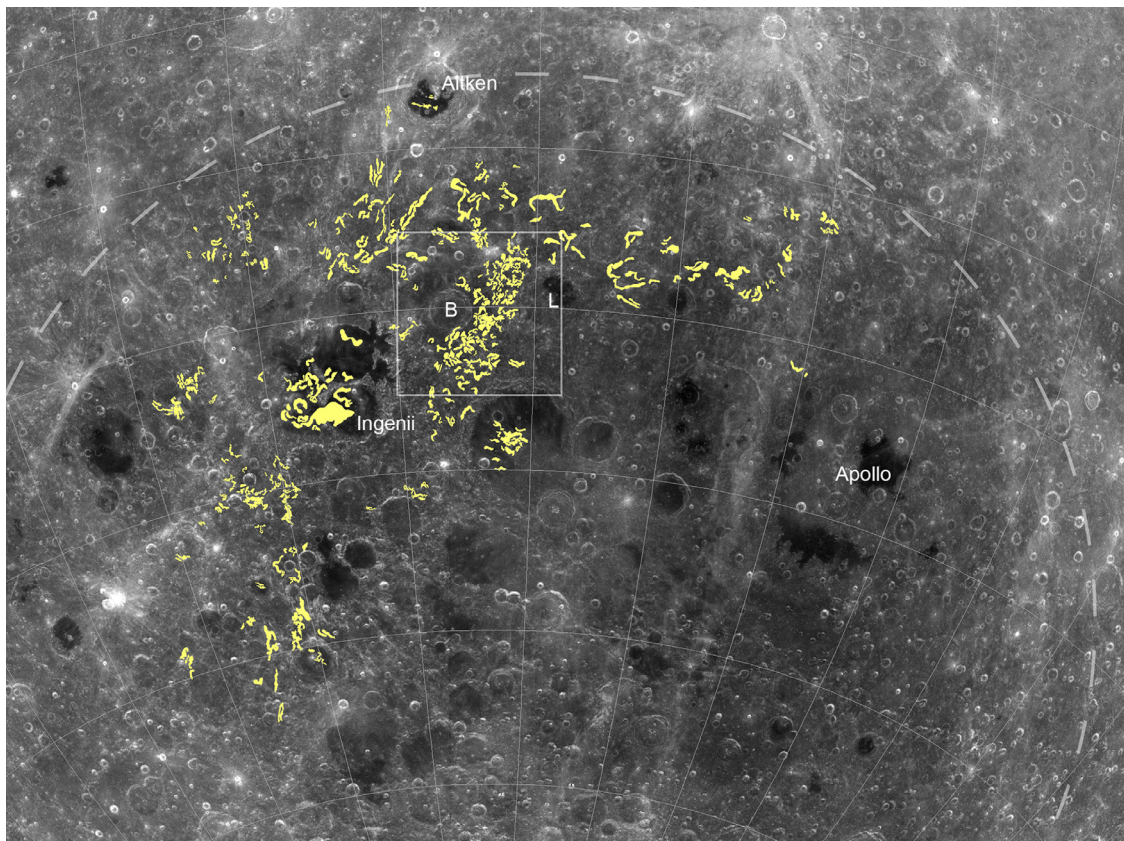


Fig. 4. View of the SPA swirl group, shown in yellow on a WAC 643 nm reflectance map, orthographically projected to a center latitude and longitude of 36°S, 177°E. Dashed line shows the approximate extent of the SPA basin, box indicates location of [Fig. 5](#). Labeled features include Birkeland crater (B) and Leeuwenhoek crater (L). Grid lines are placed every 10° of latitude and longitude.

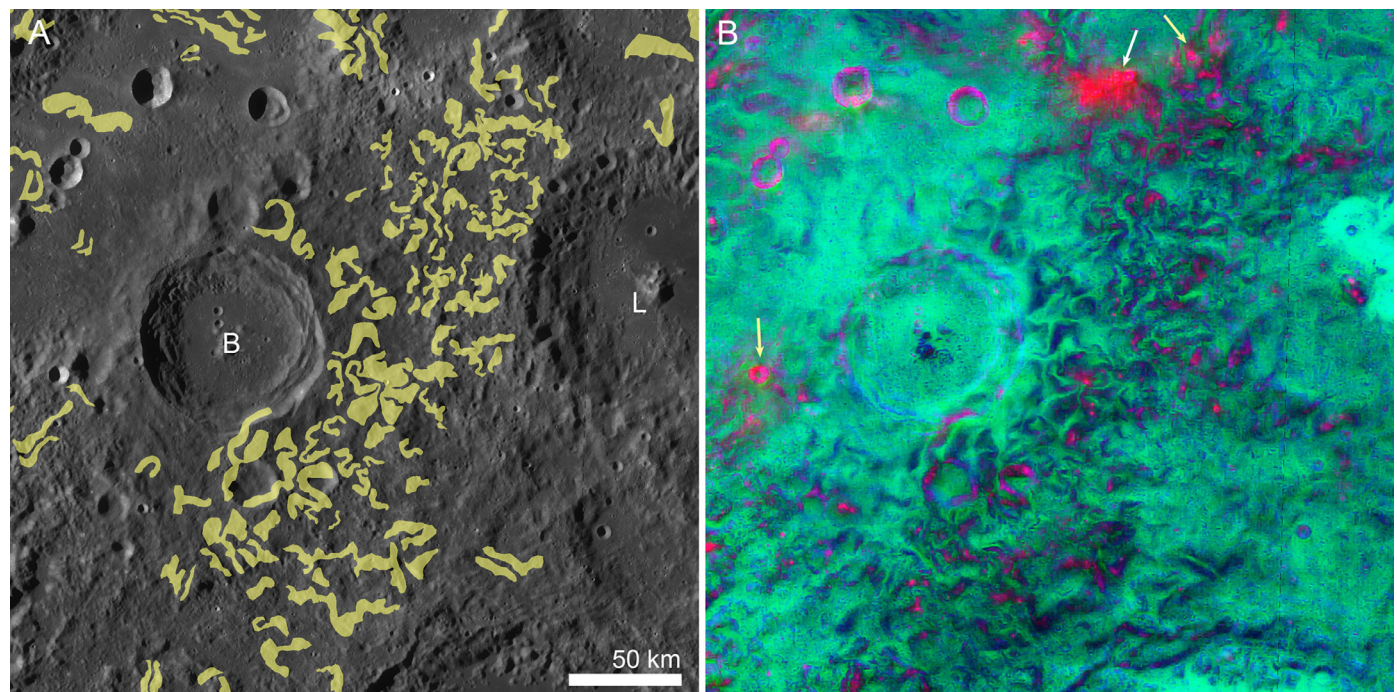


Fig. 5. Detail view of SPA swirls near Birkeland (B) and Leeuwenhoek (L) craters. A) WAC high-incidence angle map with mapped swirls shown in yellow. B) WAC color composite (415 nm, 321/415 nm, 321/360 nm in red, green, and blue). White arrow indicates a Copernican crater that appears to obscure nearby swirls. Yellow arrows indicate Eratosthenian craters; nearby swirls have distinct color properties.

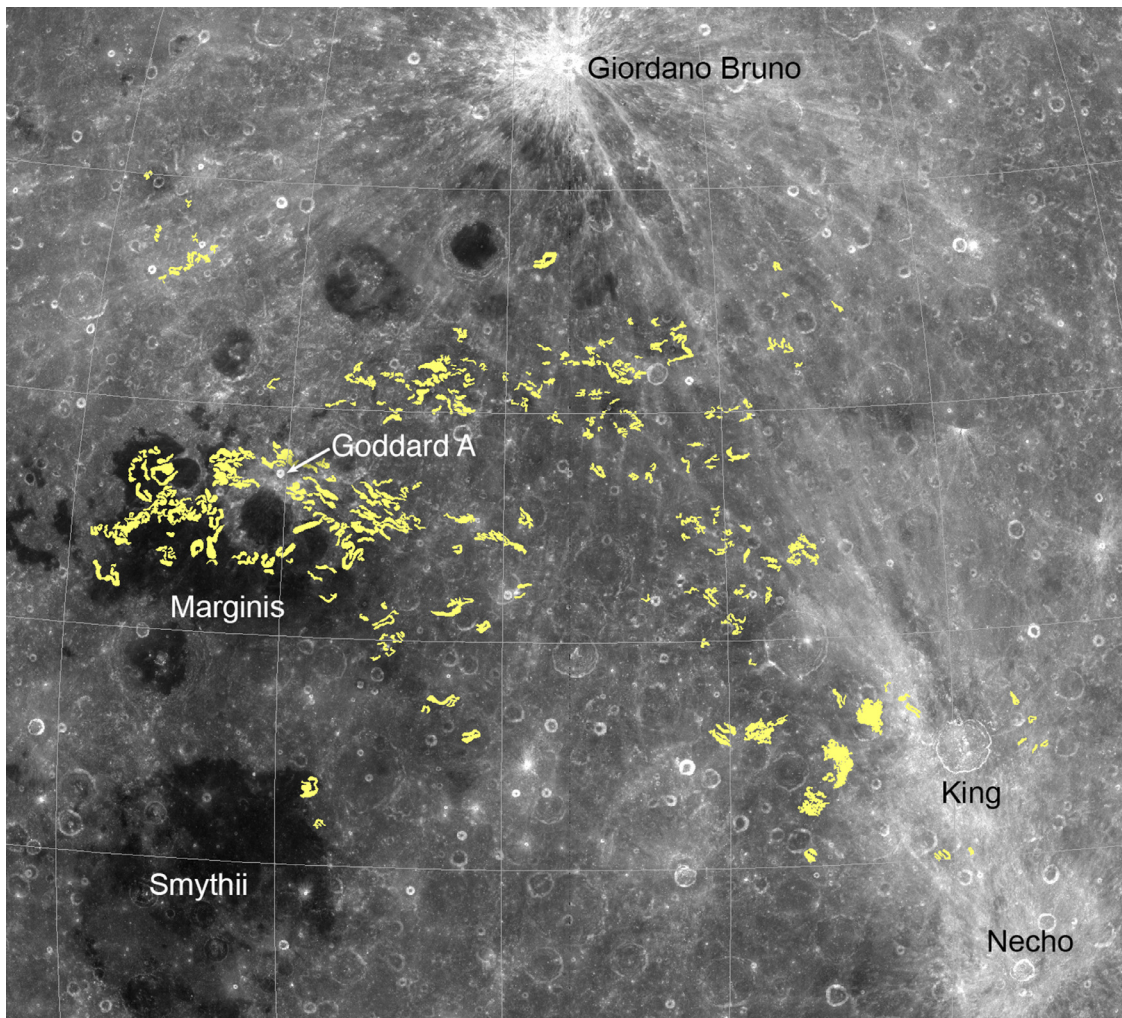


Fig. 6. View of the Marginis–King swirl group shown in yellow on a WAC 643 nm reflectance map. The region is a complex mix of swirls, maria, highlands, and the rays of fresh craters. Orthographic projection centered at 12°N, 103°E. Grid lines are placed every 10° of latitude and longitude.

3.4. Swirl characteristics

We characterized the regions in which swirls are found by examining local magnetic field strength at 30-km altitude (Richmond and Hood, 2008), iron abundance (Lawrence et al., 2002) and local topographic slope over a 1-km baseline from the GLD100 (Scholten et al., 2012). The values from each of these datasets were compared for regions within the mapped swirls to the global values as well as to the “background” values – a box selected such that it includes the regional extent of each swirl or swirl group. As previously noted, swirls are generally found in regions with higher total magnetic field strength (Fig. 10a). Globally, magnetic field strength at 30-km altitude has a narrow distribution that peaks at 0.5 nT. The swirl background regions have more broadly distributed histogram that peaks at 1.1 nT, and the swirls themselves have a broader distribution still with a mode of 3.0 nT. The minimum total magnetic field value within a swirl is 0.56 nT, compared to 0.12 nT for the swirl background region; the maximum within a swirl is 23.8 nT compared with 26.3 nT for the background.

While swirls occur throughout the highlands and maria, the Lunar Prospector-derived FeO abundance (Lawrence et al., 2002) is shifted to higher values where they are found as compared to both the global and background values (Fig. 10b). The mode of the FeO content within swirls is 7.6 wt%, compared with a background mode of 6.0 wt% and a mode of 5.6 wt% globally. The min-

imum background value is 3.5 wt% FeO and the minimum value within the swirls is 5.1 wt%. No difference is seen between the 1-km slopes where swirls occur vs. the background (Fig. 10c).

As described in Section 1, swirls exhibit distinct spectral parameters; we examine several of these in detail here. Examples are shown in Fig. 11 for Reiner Gamma, though the observations for Reiner Gamma extend generally to the other swirls mapped in this work. The WAC 321/415 nm ratio values of the swirls are lower than their surroundings in all cases, as indeed it was this parameter that was used in part to identify the swirls. This is true even for the smaller swirl features that are often slightly lower in reflectance, such as those that extend to the southwest of the main Reiner gamma feature (Fig. 11a and b). While the swirls have lower 321/415 nm ratios than their surroundings, the values of those ratios mostly vary with background composition (Fig. 12a).

Optical maturity, or OMAT, is a unitless parameter calculated from Clementine 750 and 950 nm reflectance (Lucey et al., 2000), and higher values are consistent with more immature soils. The histogram of OMAT values for the swirls is shifted to higher values (+0.02) compared to the background (Fig. 12b, mode of 0.18 vs. 0.16). Swirls cover much of the same range of OMAT values as the background terrain, except for the lowest values. However, some swirls are not readily distinguished in OMAT. For example, the smaller features to the southwest of the main Reiner Gamma swirl are not visible in the OMAT image (Fig. 11c).

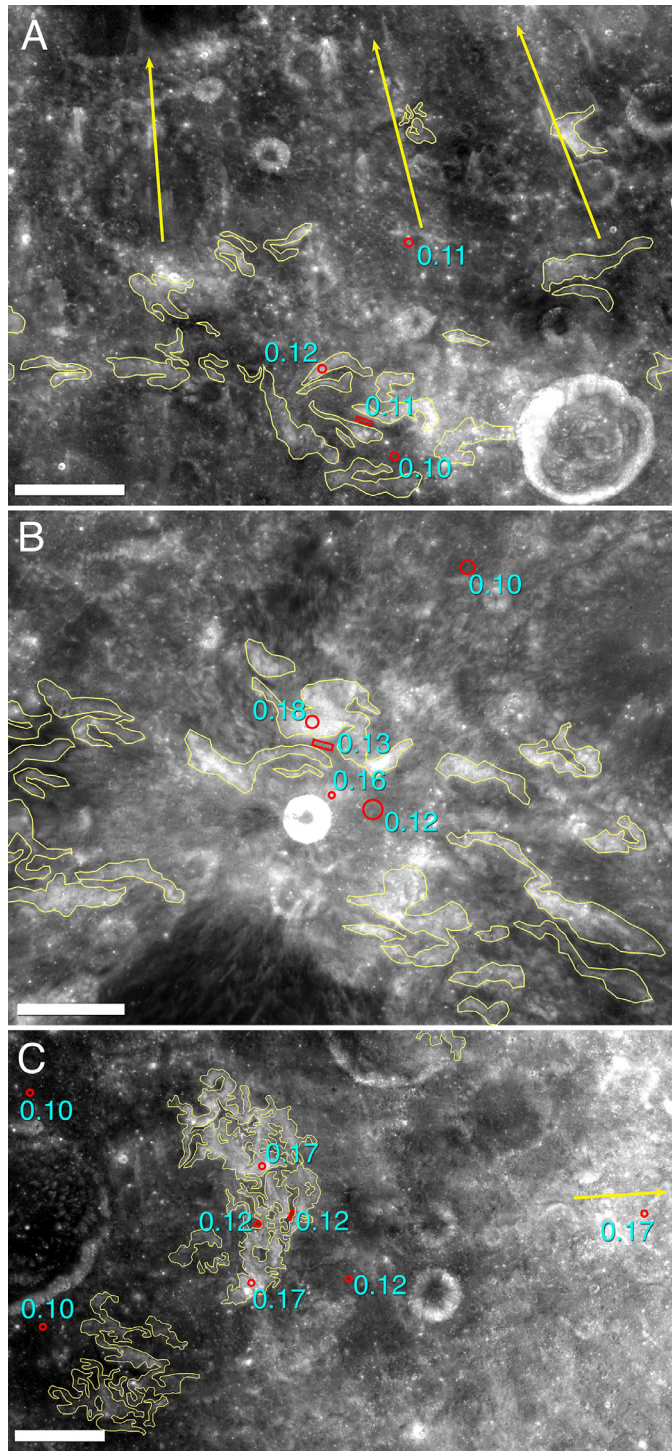


Fig. 7. Reflectance values for selected features in the Marginis-King swirl group and fresh impact craters. Swirls are outlined in yellow; photometrically corrected reflectance values at 643 nm are shown in blue type for each area indicated in red. For each example, reflectance values within swirls are similar to, or slightly higher than, reflectance within crater rays. The reflectance of inter-swirl regions ("dark lanes") is comparable to or slightly higher than background areas. (A) Swirls north of Mare Marginis, with Giordano Bruno rays (arrows). Scene centered at 23°N, 105°E. (B) Swirls north of Mare Marginis and crater Goddard A (center). Scene centered at 18°N, 90°E. (C) Firsov swirl and King ejecta (King is located just outside of the image in the direction of the arrow). Scene centered at 3°N, 116°E. Each scene is stretched independently to enhance local contrast; all scale bars are 25 km in length.

Several spectral parameters were calculated from M³ data to compare the swirls to their background. Integrated 1 and 2 μm band depths were examined; these measure the total band depth across the mafic crystal-field absorptions (see equations in Mustard et al., 2011). The swirls often have stronger 1-μm bands, although as with OMAT, the smaller features are not discernable in the integrated band depth images (Fig. 11d). The histogram of integrated 1-μm band depths is shifted to larger values for the swirls compared to the background; few swirls are found with the smallest band depth seen in the background (Fig. 12c). Swirls are barely discernable in images of integrated 2-μm band depth (Fig. 11e) and the distribution of 2 μm band depths is not clearly distinct from the background.

We also calculated a continuum slope from M³ reflectance normalized to unity at 701 nm:

$$C_n = \frac{R_{n,1579} - R_{n,701}}{1579 - 701}$$

where R_n is the normalized reflectance at 1579 and 701 nm. The swirls often but not always appear distinct in normalized continuum slope images. When they are distinct, it is because they have shallower normalized continuum slopes (Fig. 11f). The distribution of continuum slopes reflects this observation, with a mode shifted to lower slope values compared to the background (Fig. 12d).

4. Discussion

The view of the broad-scale distribution of swirls is informative. Consistent with previous work, all of the swirls we have identified here are associated with magnetic anomalies, but not all magnetic anomalies have swirls. The magnetic anomaly in the SPA basin, for example, extends further to the northeast than the swirls themselves (Fig. 3). No swirls are identified at the magnetic anomalies to the east and south of Orientale, and while a swirl is found at the small anomaly near Dufay X crater, none are found at the larger anomalies just to the east (Fig. 3). Why do some magnetic anomalies lack swirls? There could be some relationship with the native FeO content of the location. The magnetic anomalies with no swirls tend to be in low-iron regions; all except for the area south of Orientale are in the 4–5 wt% FeO range, while the swirls are generally shifted toward higher iron abundances (Fig. 11b). However, the swirls at Dufay X and Gerasimovich are found in locations with ~5 wt% FeO, so it is clearly not impossible for swirls to form in low-iron areas. If there were some mechanism by which swirl formation is impeded in regions with low iron, this would be in conflict with the comet formation model, which should be independent of local composition.

Another interesting observation is that swirls are not always especially high in reflectance, OMAT, band depth, or low in normalized continuum slope (Figs. 11 and 12) compared to their surroundings. In fact, for portions of swirls that are relatively low in reflectance, these characteristics cannot always be used to distinguish the swirls from their surroundings at all (see smaller portions of Reiner Gamma in southwestern portion of Fig. 11c, d, and f), though they can clearly be identified by their low UV ratio values (Fig. 11b). We looked for a correlation between these spectral parameters and magnetic field strength, but could not find one (the relatively low resolution of the magnetic data, however, likely prevents this analysis from being definitive). While the swirls more frequently have higher OMAT and band depth values and shallower normalized continuum slopes, they span most of the range of values seen in their regional backgrounds (Fig. 12). This is consistent with the portions of swirls that are more diffuse and lower in reflectance, and only clearly identifiable by their low UV ratio, being nearly optically mature.

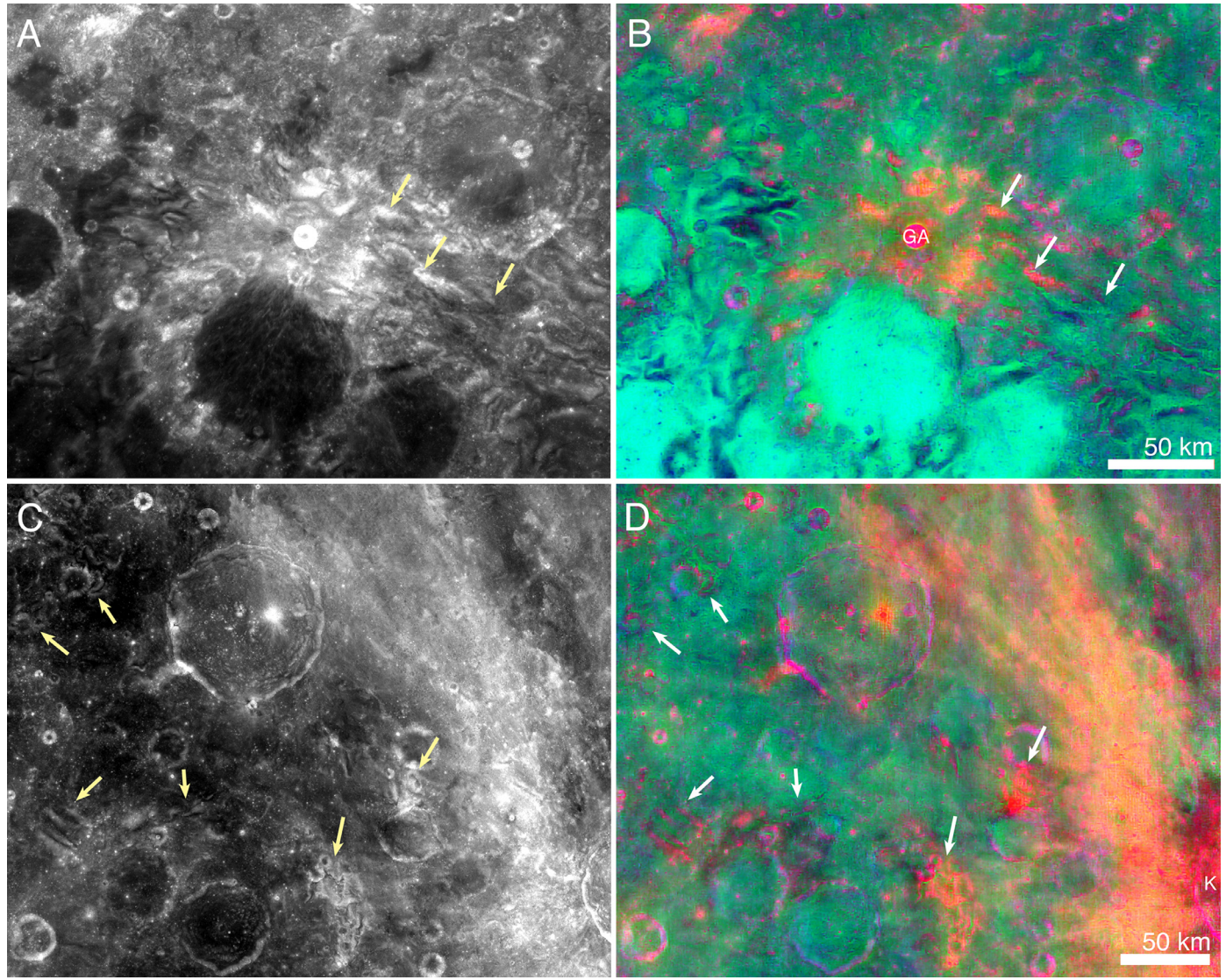


Fig. 8. Details of reflectance (643 nm) and color variation (415 nm, 321/415 nm, 321/360 nm in red, green, and blue) across swirls with distance from craters. Swirls near crater Goddard A are shown in panels A and B; swirls near King crater are shown in panels C and D. Arrows indicate examples of rays with varying color properties at increasing distances from Goddard A and King.

Since these visible and near-infrared reflectance-based parameters are not always distinct at swirls, the most distinguishing reflectance characteristic of swirls is their low UV ratio (321/415 nm) coupled with a moderate to high albedo. These two parameters are attributes of immaturity, but the steep UV slope of fresh silicates is thought to shallow more rapidly with space weathering than spectral changes that occur at longer wavelengths (Hendrix and Vilas, 2006; Hendrix et al., 2012; Denevi et al., 2014), which is apparently inconsistent with observations at the swirls. Either the UV characteristics do not change more rapidly than the visible and near-infrared characteristics with exposure to space weathering (and instead change more slowly), or the low 321/415 nm ratio values at swirls cannot be fully explained by the exposure of immature material.

Glass has strong UV absorptions consistent with the UV properties of swirls (Wells and Hapke, 1977), and the strength of these absorptions could explain why the UV properties are so distinct even for diffuse and faint swirls. However, glass also has distinct spectral characteristics across the visible and near-infrared including 1- and 2- μm crystal field absorptions that are broader than those of pyroxenes, and depending on composition, often a

strong peak in reflectance near 700 nm (Bell et al., 1976; Wells and Hapke, 1977). Denevi et al. (2014) examined WAC spectra of Reiner Gamma and found no indication of glass at visible wavelengths. It is possible that this contradiction could be reconciled by considering the strength of the absorption features. The charge-transfer absorption responsible for the UV properties is much stronger than the crystal-field absorption responsible for the visible and near-infrared absorptions (Bell et al., 1976; Wells and Hapke, 1977); it is thus plausible that glass in a mixture (with silicate minerals) could affect the ultraviolet properties of the spectrum with a much smaller effect on the visible–near-infrared reflectance. Agglutinite glass does not share the spectral properties described above for glass due to the embedded submicroscopic iron within its volume; agglutinates are low in reflectance with a shallow spectral slope (Pieters et al., 1993) due to relatively large grains of embedded submicroscopic iron (Keller et al., 1998; Hapke, 2001; Keller and Clemett, 2001; James et al., 2002; Basu, 2005). If glass is responsible for the spectral properties observed at swirls, it could either be large-scale impact glass (possibly consistent with the comet model), or glass produced in a similar manner to agglutinates, but without the high abundance of submicroscopic

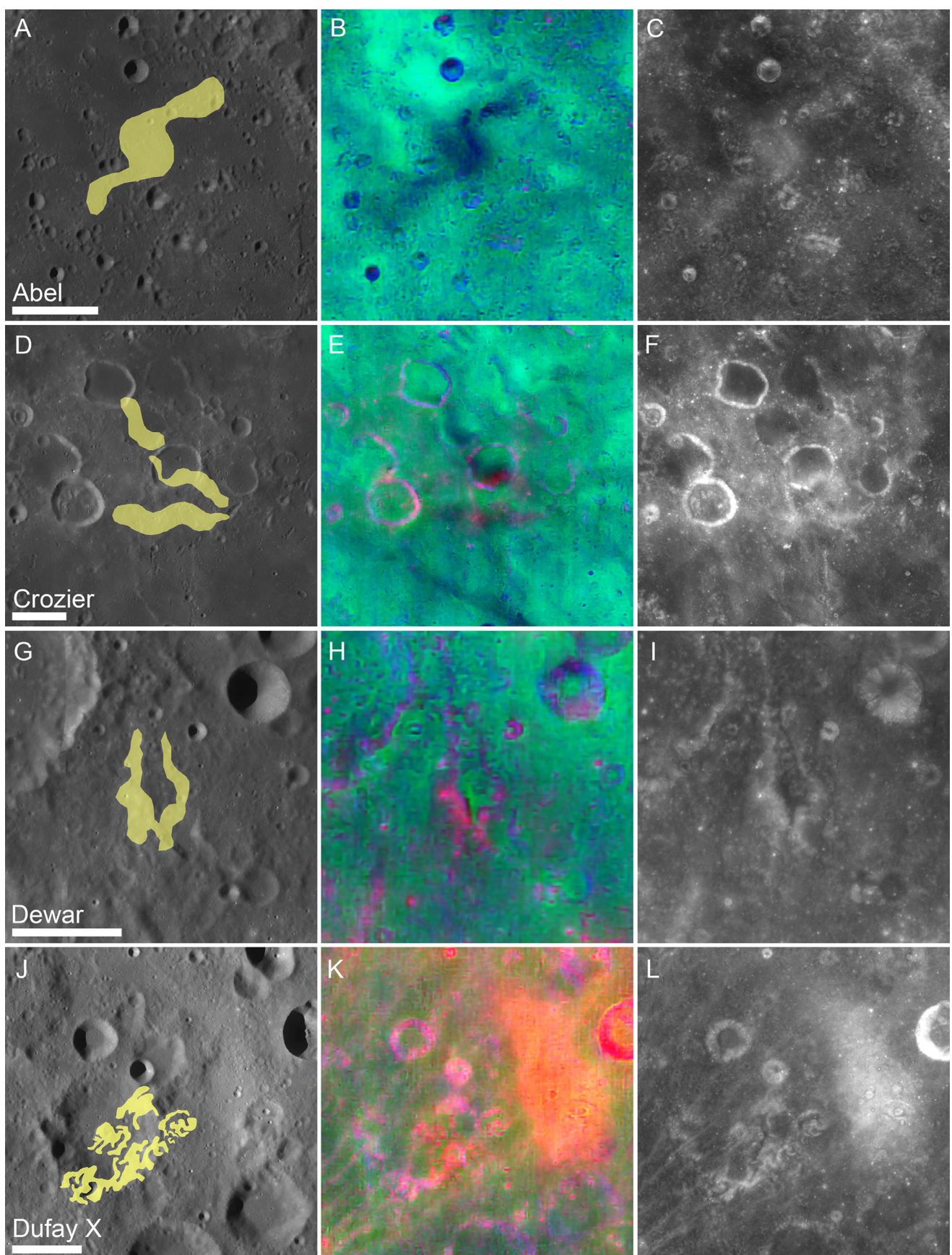


Fig. 9. Swirls identified in this work at the magnetic anomalies near Abel crater (A–C; centered at 36.7°S, 89.1°E), Crozier crater (D–F, centered at 15.0°S, 51.5°E), Dewar crater (G–I, centered at 3.5°S, 166.9°E), and Dufay X crater (J–L, centered at 7.1°N, 169.0°E). The left panel for each feature shows the mapped swirl extent on a high-incidence map to highlight regional morphology, the center panel is the WAC color composite (415 nm, 321/415 nm, 321/360 nm in red, green, and blue), and the right panel is the WAC 643 nm reflectance. Each scale bar is 25 km.

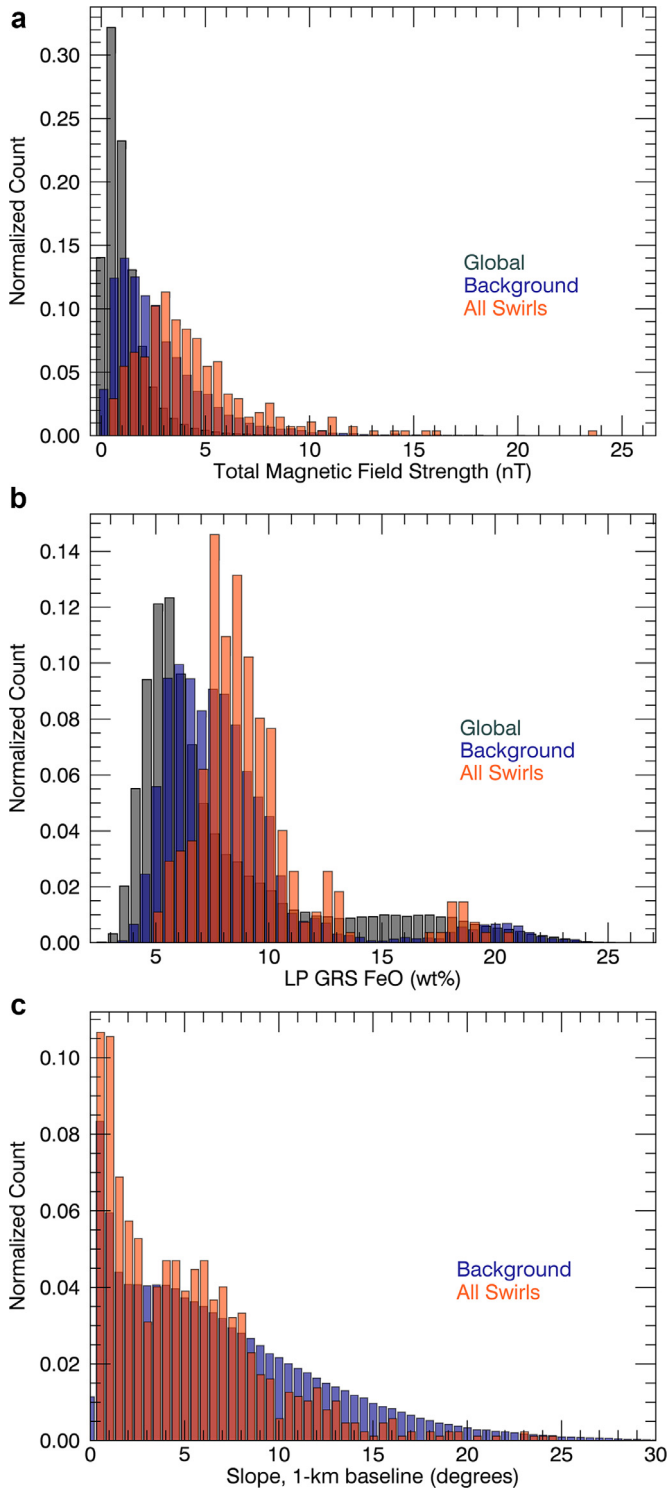


Fig. 10. (A) Histogram of the total magnetic field strength continued to 30 km altitude (Richmond and Hood, 2008) for the whole Moon (global), swirls, and regional setting for the swirls (background). (B) Lunar Prospector-derived FeO abundance (Lawrence et al., 2002). (C) Slopes over a 1-km baseline as calculated from the GLD100 (Scholten et al., 2012). Counts were collected from a sinusoidal projection where every pixel is equal in area, and each histogram is normalized to the total number of pixels.

iron (micrometeoroid bombardment without a large contribution of sputtered iron from the solar wind, and without implanted hydrogen incorporated into the melt, see discussion of agglutinate formation in Basu (2005)). The sorting models (either enrichment of dust (Garrick-Bethell et al., 2011) or depletion of the magnetic fraction (Pieters and Garrick-Bethell, 2015)) do not account for a larger glassy fraction in the swirls, if indeed the UV signatures are due to glass. Regardless of whether the UV properties of swirls are due to the exposure of fresh silicates or are due to the presence of glass, the observations presented in this work are consistent with a dearth of agglutinates within the swirls. This is true whether the submicroscopic-iron-bearing agglutinates were never produced, or if they were produced but removed by magnetic sorting.

WAC color composites reveal interesting relationships between swirls and nearby fresh craters. Continuous ejecta deposits of fresh craters do appear to superpose swirls (Fig. 5d), in some cases completely obscuring them. In other cases, swirl color is clearly affected by nearby fresh craters (Fig. 5d and 7). We find the case of the Eratosthenian craters in Fig. 5d to be the most thought provoking. Though the craters no longer displays fresh ejecta or rays, the swirls in their immediate vicinity have color properties associated with fresh ejecta elsewhere. Could this be a case where the ejecta deposits from these craters were preserved as fresh within the swirls, but were space weathered to maturity outside of the swirls? This case is consistent with the solar wind shielding model, and suggests that swirls can indeed be “refreshed” with the ejecta of nearby craters (Hood et al., 1979b, 2001; Blewett et al., 2011).

The photometry of the swirls is a tantalizing clue to their origin, but unfortunately does not point to an obvious answer for their formation. The forward scattering nature of the swirls, which is distinct from the photometric behavior of fresh craters, was interpreted in terms of a lower roughness or higher compaction (Schultz and Srnka, 1980; Pinet et al., 2000; Kreslavsky and Shkuratov, 2003; Kaydash et al., 2009), and taken as consistent with the comet model for swirl formation. However, roughness or compaction differences are apparently ruled out by the completely typical thermophysical properties of the swirls (Glotch et al., 2015). Other properties also affect the phase function of a soil, including grain shape, internal scattering (caused by inclusions, defects, and boundaries inside particles), and albedo (McGuire and Hapke, 1995). Sato et al. (2014) suggest the complex agglutinate grains could have a large control on the scattering behavior of the lunar surface, and are dominantly backscattering, as opposed to transparent silicates, which are forward scattering. However, Sato et al. find that fresh impact craters are strongly backscattering and attribute this characteristic to the presence of optically thick cobbles and rocks. The forward-scattering nature of the swirls could be the case where transparent silicates are exposed, without a large agglutinate population and without larger clasts that would reduce forward scattering. Radar observations of swirls confirm that soils at swirls are of similar grain size to typical soils, without a rocky component (Neish et al., 2011). The photometric properties of swirls merit further study, but may also be pointing to a lack of submicroscopic-iron-bearing agglutinates.

After reviewing the evidence described above, we conclude it is premature to definitively rule in favor of any one model for formation of swirls, though a preponderance of the evidence leans toward the solar wind shielding hypothesis. The strongest additional support that we provide in this work, is the associations with small Copernican and Eratosthenian crater ejecta. We see no obvious mechanism by which the comet or sorting models could result in maturity variations within swirls that are related to distance from small Eratosthenian craters. Solar wind shielding of portions of the ejecta (areas within the margins of swirls) could result in some ejecta remaining fresh while the rest matures. However if some variant of the solar wind shielding model is correct, it does appear

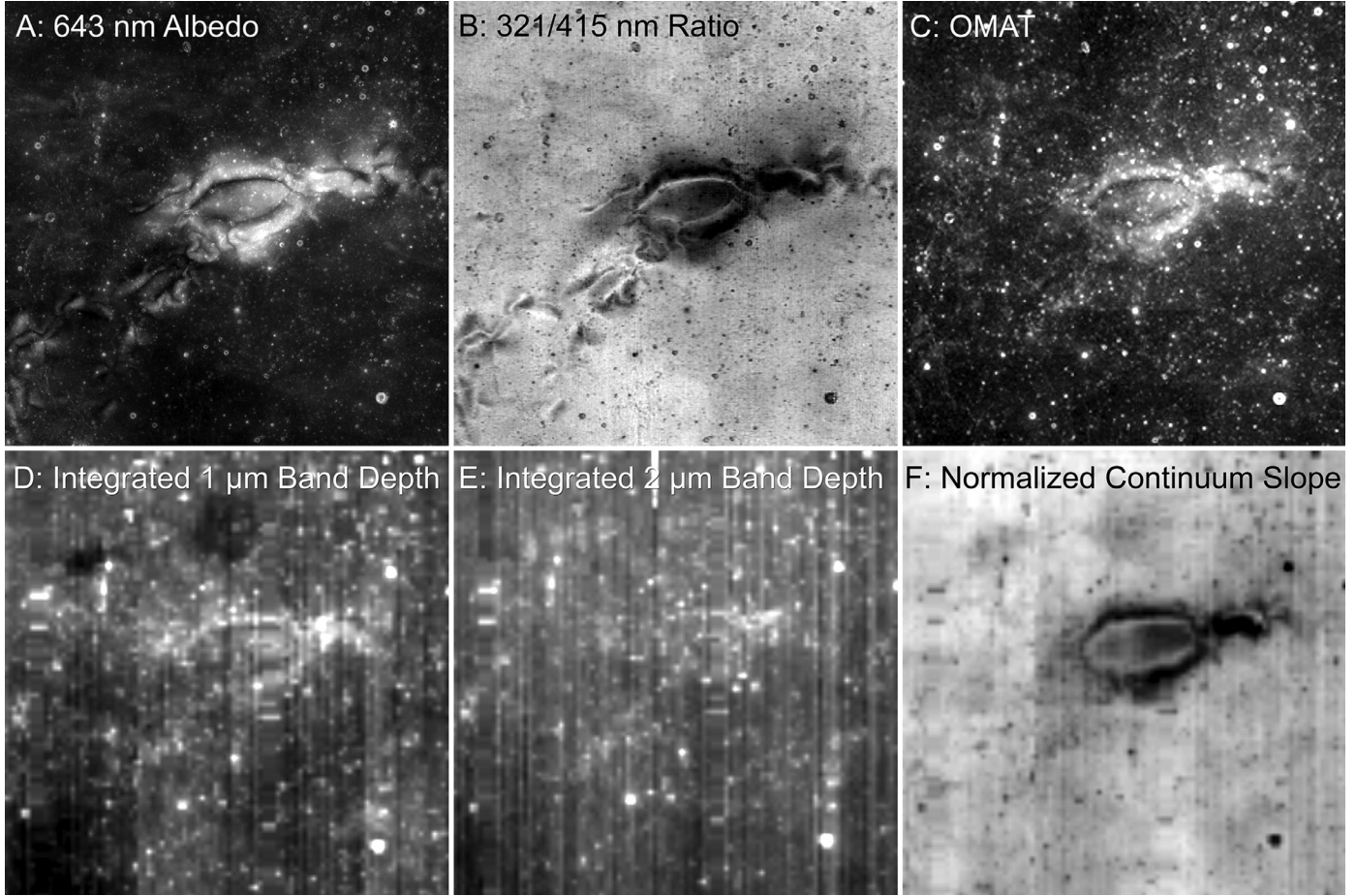


Fig. 11. Example spectral parameters for the Reiner Gamma swirl. Each panel is approximately 145 km across.

that the swirls “mature” to some extent, consistent with previous work (e.g., Blewett et al., 2011; Kramer et al., 2011a; Hemingway et al., 2015). WAC UV observations indicate that swirls far from fresh craters are distinct from swirls near fresh craters, and from fresh craters themselves (e.g., Fig. 8). This difference with fresh craters could indicate that swirls reach a steady state of maturation that is distinct from typical mature soils, consistent with the observations of Hemingway et al. (2015). Part of the difference from typical mature soils could be due to either a lack of agglutinates or agglutinates that do not have large embedded submicroscopic iron grains (and thus their spectral signature is dominated by glass rather than metallic iron). If the solar wind shielding hypothesis is correct, this observation points to the importance of a pre-existing population of nanophase iron from solar wind sputtering, and/or implanted solar wind, in creating typical low-reflectance agglutinates.

5. Conclusions

We mapped the distribution of swirls across the lunar surface using LROC WAC color composite images. The most distinguishing characteristics of swirls are their low 321/415 nm ratios coupled with moderate to high reflectance. Two large geographic groupings of swirls are mapped, one that occupies the northwestern portion of the SPA basin, and another that extends from Mare Marginis to King crater. We have identified many more swirls in SPA, so that they are revealed to extend nearly continuously across the region rather than the more discrete patches described previously around Ingenii, Hopmann, and northwest of the Apollo basin. We

find little difference with previous maps (Schultz and Srnka, 1980) for the Marginis–King region. Other smaller clusters of swirls or individual swirls are similar to those described in Blewett et al. (2011), with the addition of newly identified features at Abel, Crozier, Dewar, and Dufay X.

Consistent with previous work, swirls are associated with magnetic anomalies, though not all magnetic anomalies have swirls. Swirls are generally found in areas with iron contents that are higher than their surroundings and shifted to higher values compared to the global FeO distribution (Fig. 10b). Magnetic anomalies that lack swirls tend to be in lower iron areas.

In addition to their albedo and UV characteristics, swirls have OMAT values and 1-μm band depths that are shifted to slightly higher values than their surroundings, and shallower continuum slopes (Fig. 12). However, swirls with only moderately elevated reflectance are often barely distinguishable in OMAT, band depth, or continuum images. This is in contrast to their 321/415 nm ratios, which are distinct even when these other parameters are not (Fig. 11).

Swirl color properties vary with distance from Copernican and some Eratosthenian craters; near these craters, swirls have lower UV ratios, higher reflectance, and higher OMAT values. The association with Eratosthenian craters suggests fresh material exposed by impact craters may be preserved for a longer duration within swirls, as opposed to in non-swirl areas of the ejecta deposit. The difference between typical swirls and Copernican crater ejecta implies that the majority of swirls have reached some degree of maturity or have some other property that results in spectral characteristics that are distinct from those of fresh craters.

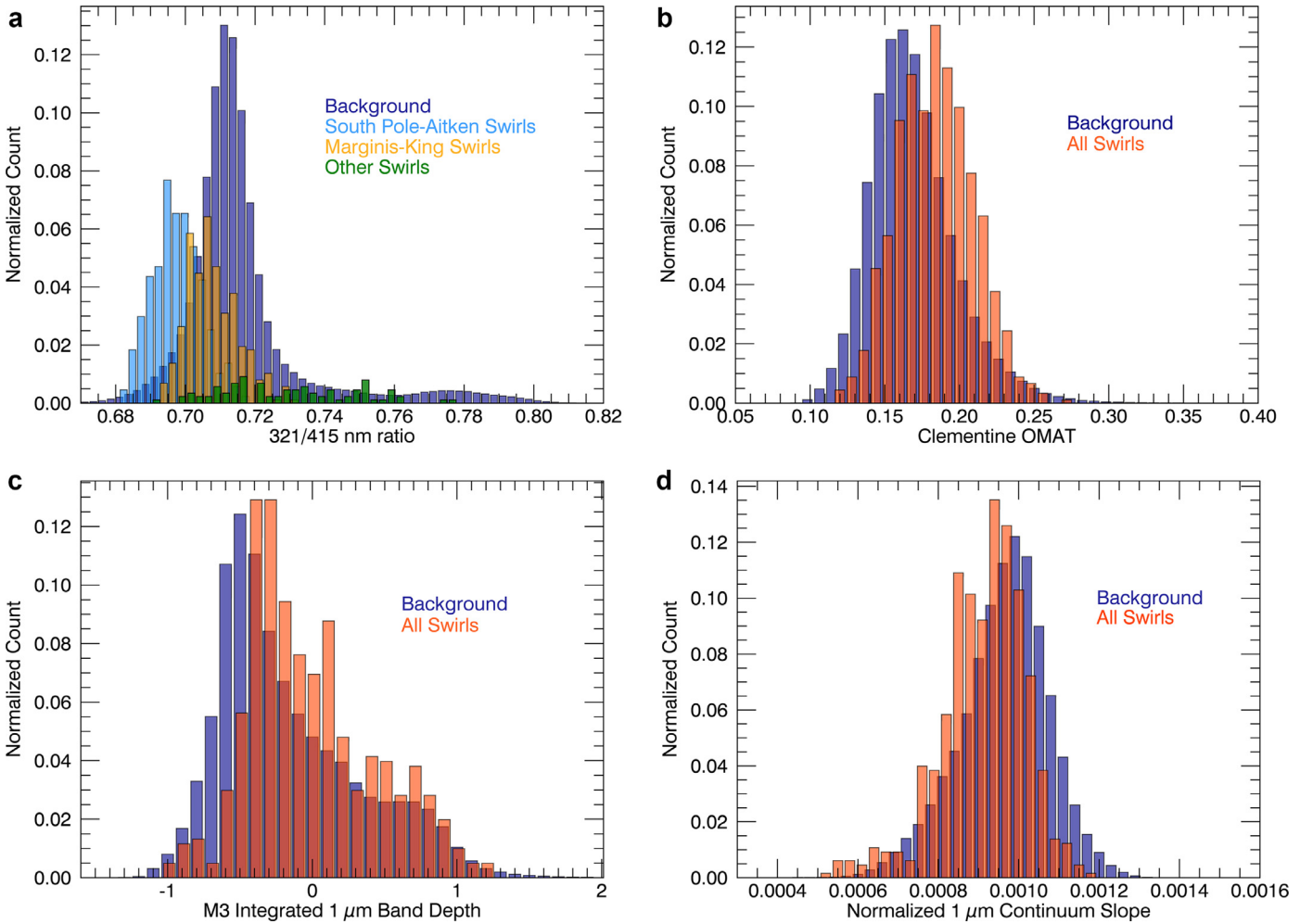


Fig. 12. Spectral characteristics of lunar swirls. (A) WAC 321/415 nm ratio for the swirls in comparison to the background. (B) Clementine-derived optical maturity (OMAT) (Lucey et al., 2000) of swirls and background. (C) M³-derived integrated 1 μm band depth (Mustard et al., 2011). (D) M³-derived normalized continuum slope. Counts were collected from a sinusoidal projection where every pixel is equal in area, and each histogram is normalized to the total number of pixels (swirls in A are normalized to their combined total).

The low UV ratios for swirls could be related to the exposure of fresh silicates or the presence of a glassy component that does not have a substantial fraction of large embedded submicroscopic iron grains. Such glass could be the product of micrometeorite bombardment in an environment with reduced or absent solar wind sputtering and/or a lack of implanted solar wind, i.e., a difference in the agglutinates fraction of the soil.

Taken together, the work here in conjunction with findings from previous studies is most consistent with the solar wind shielding hypothesis for swirl formation, though we look forward to further consideration of magnetic sorting. However, without new observations, it may not be possible to arrive at a definitive consensus on the nature of the swirls. Thus we end here with the words of Whitaker (1969), in discussing Lunar Orbiter and Apollo 8 photographs of the swirls at Mare Ingenii and Marginis: “Clearly, more work needs to be done before any firm conclusions can be drawn.” In this case, more work should include magnetic measurements at the spatial scale of the high- and low-reflectance portions of swirls (Robinson et al., 2015), and surface characterization of local soil chemical and physical properties and solar wind characteristics.

Acknowledgments

We thank Lon Hood for helpful discussions and reviewers Ed Cloutis and Georgiana Kramer for their reviews. This work was

supported by the National Aeronautics and Space Administration Lunar Reconnaissance Orbiter Project contract NNG07EK00C. D.T.B. is supported by NASA Lunar Advanced Science and Exploration Research Program grant NNX14AQ91G. This research makes use of the USGS Integrated Software for Imagers and Spectrometers (ISIS). We wish to thank Kris Becker and Jeff Anderson at the USGS Astrogeology Center in Flagstaff for their support in developing the tools to process and analyze LROC WAC data. LROC data are archived in the Planetary Data System.

Supplementary materials

Supplementary material associated with this article can be found, in the online version, at doi:10.1016/j.icarus.2016.01.017.

References

- Adams, J.B., McCord, T.B., 1973. Vitrification in the lunar highlands and identification of Descartes material at the Apollo 16 site. In: Proceedings of the 4th Lunar Science Conference, pp. 163–177.
- Basu, A., 2005. Nanophase Fe⁰ in lunar soils. *J. Earth Syst. Sci.* 114 (3), 375–380.
- Bell, J.F., Hawke, B.R., 1981. The Reiner Gamma formation: Composition and origin as derived from remote sensing observations. In: Proceedings of 12th Lunar Planetary Science, pp. 679–694.
- Bell, J.F., Hawke, B.R., 1987. Recent comet impacts on the Moon: The evidence from remote-sensing studies. *Publ. Astron. Soc. Pac.* 99, 862–867.

- Bell, P.M., Mao, H.K., Weeks, R.A., 1976. Optical spectra and electron paramagnetic resonance of lunar and synthetic glasses: A study of the effects of controlled atmosphere, composition, and temperature. In: Proceedings of 7th Lunar Science Conference, pp. 2543–2559.
- Blewett, D.T., 2005. Lunar optical maturity investigations: A possible recent impact crater and a magnetic anomaly. *J. Geophys. Res.* 110 (E4). doi:[10.1029/2004JE002380](https://doi.org/10.1029/2004JE002380).
- Blewett, D.T., Denevi, B.W., Robinson, M.S., et al., 2010. The apparent lack of lunar-like swirls on Mercury: Implications for the formation of lunar swirls and for the agent of space weathering. *Icarus* 209 (1), 239–246. doi:[10.1016/j.icarus.2010.03.008](https://doi.org/10.1016/j.icarus.2010.03.008).
- Blewett, D.T., Coman, E.I., Hawke, B.R., et al., 2011. Lunar swirls: Examining crustal magnetic anomalies and space weathering trends. *J. Geophys. Res.* 116 (E02002). doi:[10.1029/2010JE004656](https://doi.org/10.1029/2010JE004656).
- Boardman, J.W., Pieters, C.M., Green, R.O., et al., 2011. Measuring moonlight: An overview of the spatial properties, lunar coverage, selenolocation, and related Level 1B products of the Moon mineralogy mapper. *J. Geophys. Res. Planets* 116 (E6). doi:[10.1029/2010JE003730](https://doi.org/10.1029/2010JE003730).
- Boyd, A.K., Robinson, M.S., Sato, H., 2012. Lunar reconnaissance orbiter wide angle camera photometry: An empirical solution. *Lunar Planetary Science* 43, Abstract 2795.
- Bruck Syal, M., Schultz, P.H., 2015. Cometary impact effects at the Moon: Implications for lunar swirl formation. *Icarus* 257, 194–206. doi:[10.1016/j.icarus.2015.05.005](https://doi.org/10.1016/j.icarus.2015.05.005).
- Coman, E.I., Blewett, D.T., Hawke, B.R., et al., 2011. Lunar swirls: How dark are “dark lanes”. *Lunar Planetary Science Conference* 42, Abstract 1096.
- Crawford, D.A., Schultz, P.H., 1999. Electromagnetic properties of impact-generated plasma, vapor and debris. *Int. J. Impact Eng.* 23, 169–180. doi:[10.1016/S0734-743X\(99\)00070-6](https://doi.org/10.1016/S0734-743X(99)00070-6).
- Denevi, B.W., Robinson, M.S., Boyd, A.K., et al., 2014. Characterization of space weathering from Lunar Reconnaissance Orbiter Camera ultraviolet observations of the Moon. *J. Geophys. Res. Planets* 119 (5). doi:[10.1002/2013JE004527](https://doi.org/10.1002/2013JE004527).
- El-Baz, F., 1972. *Apollo 16 Preliminary Science Report*, NASA SP-315 29–93–29–97.
- Garrick-Bethell, I., Head, J.W., Pieters, C.M., 2011. Spectral properties, magnetic fields, and dust transport at lunar swirls. *Icarus* 212 (2), 480–492. doi:[10.1016/j.icarus.2010.11.036](https://doi.org/10.1016/j.icarus.2010.11.036).
- Glotch, T.D., Bandfield, J.L., Lucey, P.G., et al., 2015. Formation of lunar swirls by magnetic field standoff of the solar wind. *Nat. Commun.* 6, 6189. doi:[10.1038/ncomms7189](https://doi.org/10.1038/ncomms7189).
- Gold, T., Soter, S., 1976. Cometary impact and the magnetization of the Moon. *Planet. Space Sci.* 24 (1), 45–54. doi:[10.1016/0032-0633\(76\)90060-X](https://doi.org/10.1016/0032-0633(76)90060-X).
- Grier, J.A., McEwen, A.S., Lucey, P.G., et al., 2001. Optical maturity of ejecta from large rayed lunar craters. *J. Geophys. Res.-Planet* 106 (E12), 32847–32862.
- Halekas, J.S., Delory, G.T., Brain, D.A., et al., 2008. Density cavity observed over a strong lunar crustal magnetic anomaly in the solar wind: a mini-magnetosphere? *Planet. Sp. Sci.* 56 (7), 941–946. doi:[10.1016/j.pss.2008.01.008](https://doi.org/10.1016/j.pss.2008.01.008).
- Hapke, B., 2001. Space weathering from Mercury to the asteroid belt. *J. Geophys. Res.* 106 (E5), 10039–10073.
- Hemingway, D., Garrick-Bethell, I., 2012. Magnetic field direction and lunar swirl morphology: Insights from Airy and Reiner Gamma. *J. Geophys. Res.* 117 (E10), E10012. doi:[10.1029/2012JE004165](https://doi.org/10.1029/2012JE004165).
- Hemingway, D.J., Garrick-Bethell, I., Kreslavsky, M.A., 2015. Latitudinal variation in spectral properties of the lunar maria and implications for space weathering. *Icarus* 261, 66–79. doi:[10.1016/j.icarus.2015.08.004](https://doi.org/10.1016/j.icarus.2015.08.004).
- Hendrix, A.R., Vilas, F., 2006. The effects of space weathering at UV wavelengths: S-class asteroids. *Astron. J.* 132, 1396–1404.
- Hendrix, A.R., et al., 2012. The lunar far-UV albedo: Indicator of hydration and weathering. *J. Geophys. Res.* 117 (E12), E12001. doi:[10.1029/2012JE004252](https://doi.org/10.1029/2012JE004252).
- Hendrix, A.R., et al., 2015. Far-ultraviolet characteristics of lunar swirls. In: Proceedings of Lunar Planetary Science Conference 46.
- Hood, L.L., 1995. Frozen fields. *Earth Moon Planets* 67, 131–142.
- Hood, L.L., Huang, Z., 1991. Formation of magnetic anomalies antipodal to lunar impact basins: Two-dimensional model calculations. *J. Geophys. Res.* 96 (B6), 9837–9846. doi:[10.1029/91JB00308](https://doi.org/10.1029/91JB00308).
- Hood, L.L., Schubert, G., 1980. Lunar magnetic anomalies and surface optical properties. *Science* 208, 49–51.
- Hood, L.L., Williams, C.R., 1989. The lunar swirls: Distribution and possible origins. In: Proceedings of 19th Lunar Planetary Science Conference, pp. 99–113.
- Hood, L.L., Coleman, P.J., Wilhelms, D.E., 1979. Lunar nearside magnetic anomalies. In: Proceedings of 10th Lunar Planetary Science Conference, pp. 2235–2257.
- Hood, L.L., Coleman, P.J., Wilhelms, D.E., 1979. The Moon: Sources of the crustal magnetic anomalies. *Science* 204, 53–57.
- Hood, L.L., Zakharian, A., Halekas, J., et al., 2001. Initial mapping and interpretation of lunar crustal magnetic anomalies using Lunar Prospector magnetometer data. *J. Geophys. Res.* 106, 27825–27840.
- Hood, L.L., Richmond, N.C., Spudis, P.D., 2013. Origin of strong lunar magnetic anomalies: Further mapping and examinations of LROC imagery in regions antipodal to young large impact basins. *J. Geophys. Res. Planets* 118 (6), 1265–1284. doi:[10.1002/jgre.20078](https://doi.org/10.1002/jgre.20078).
- James, C., Letsinger, S., Basu, A., et al., 2002. Size distribution of Fe globules in lunar agglutininitic glass. *Lunar Planetary Science Conference* 33, Abstract 1827.
- Kaydash, V., Kreslavsky, M., Shkuratov, Y., et al., 2009. Photometric anomalies of the lunar surface studied with SMART-1 AMIE data. *Icarus* 202 (2), 393–413. doi:[10.1016/j.icarus.2009.03.018](https://doi.org/10.1016/j.icarus.2009.03.018).
- Keller, L.P., Wentworth, S.J., McKary, D.S., 1998. Space weathering: reflectance spectroscopy and TEM analysis of individual lunar soil grains. *Lunar Planetary Science* 32, Abstract 2097.
- Keller, P., Clemett, S.J., 2001. Formation of nanophasic iron in the lunar regolith. In: *Proceedings of Lunar Planetary Science Conference* 32 Abstract 2097.
- Kramer, G.Y., Combe, J.-P., Harnett, E.M., et al., 2011. Characterization of lunar swirls at Mare Ingenii: A model for space weathering at magnetic anomalies. *J. Geophys. Res.* 116 (E4), E04008. doi:[10.1029/2010JE003669](https://doi.org/10.1029/2010JE003669).
- Kramer, G.Y., et al., 2011. M3 spectral analysis of lunar swirls and the link between optical maturation and surface hydroxyl formation at magnetic anomalies. *J. Geophys. Res.: Planets* 116 (E9), E00G18. doi:[10.1029/2010JE003729](https://doi.org/10.1029/2010JE003729).
- Kreslavsky, M.A., Shkuratov, Y.G., 2003. Photometric anomalies of the lunar surface: Results from Clementine data. *J. Geophys. Res.* 108 (E3), 5015. doi:[10.1029/2002JE001937](https://doi.org/10.1029/2002JE001937).
- Lawrence, D.J., Feldman, W.C., Elphic, R.C., et al., 2002. Iron abundances on the lunar surface as measured by the Lunar Prospector gamma-ray and neutron spectrometers. *J. Geophys. Res.* 107 (E12). doi:[10.1029/2001JE001530](https://doi.org/10.1029/2001JE001530).
- Lawrence, S.J., Hawke, B.R., Gillis-Davis, J.J., et al., 2008. Composition and origin of the Dewar geochemical anomaly. *J. Geophys. Res.* 113 (E2), E02001. doi:[10.1029/2007JE002904](https://doi.org/10.1029/2007JE002904).
- Lucey, P.G., Taylor, G.J., Malaret, E., 1995. Abundance and distribution of iron on the Moon. *Science* 268, 1150–1153.
- Lucey, P.G., Blewett, D.T., Taylor, G.J., et al., 2000. Imaging of lunar surface maturity. *J. Geophys. Res.* 105 (E8), 20377–20386.
- Lue, C., Futaana, Y., Barabash, S., et al., 2011. Strong influence of lunar crustal fields on the solar wind flow. *Geophys. Res. Lett.* 38 (3), L03202. doi:[10.1029/2010GL046215](https://doi.org/10.1029/2010GL046215).
- McCauley, J.F., 1967. *Geologic Map of The Hevelius Region of The Moon*. U.S. Geological Survey, I-491.
- McGuire, A.F., Hapke, B.W., 1995. An experimental study of light scattering by large, irregular particles. *Icarus* 113, 134–155.
- Mitchell, D.L., Halekas, J.S., Lin, R.P., et al., 2008. Global mapping of lunar crustal magnetic fields by Lunar Prospector. *Icarus* 194 (2), 401–409. doi:[10.1016/j.icarus.2007.10.027](https://doi.org/10.1016/j.icarus.2007.10.027).
- Mustard, J.F., Pieters, C.M., Isaacson, P.J., et al., 2011. Compositional diversity and geologic insights of the Aristarchus crater from Moon Mineralogy Mapper data. *J. Geophys. Res.* 116 (E6), E00G12. doi:[10.1029/2010JE003726](https://doi.org/10.1029/2010JE003726).
- Neish, C.D., Blewett, D.T., Bussey, D.B.J., et al., 2011. The surficial nature of lunar swirls as revealed by the Mini-RF instrument. *Icarus* 215 (1), 186–196. doi:[10.1016/j.icarus.2011.06.037](https://doi.org/10.1016/j.icarus.2011.06.037).
- Pieters, C.M., Garrick-Bethell, I., 2015. Hydration variations at lunar swirls. *Lunar Planetary Science* 46, Abstract 2120.
- Pieters, C.M., Fischer, E.M., Rode, O., et al., 1993. Optical effects of space weathering: The role of the finest fraction. *J. Geophys. Res.* 98 (E11), 20817–20824.
- Pieters, C.M., Boardman, J., Buratti, B., et al., 2009. The Moon Mineralogy Mapper (M3) on Chandrayaan-1. *Curr. Sci.* 96 (4), 500–505.
- Pieters, C.M., Moriarty III, D.P., Garrick-Bethell, I., 2014. Atypical regolith processes hold the key to enigmatic lunar swirls. *Lunar Planetary Science* 45, Abstract 1408.
- Pinet, P.C., Shevchenko, V.V., Chevrel, S.D., et al., 2000. Local and regional lunar regolith characteristics at Reiner Gamma Formation: Optical and spectroscopic properties from Clementine and Earth-based data. *J. Geophys. Res.* 105 (E4), 9457–9475. doi:[10.1029/1999JE001086](https://doi.org/10.1029/1999JE001086).
- Richmond, N.C., Hood, L.L., 2008. A preliminary global map of the vector lunar crustal magnetic field based on Lunar Prospector magnetometer data. *J. Geophys. Res.* 113 (E2), E02010. doi:[10.1029/2007JE002933](https://doi.org/10.1029/2007JE002933).
- Richmond, N.C., Hood, L.L., Halekas, J.S., et al., 2003. Correlation of a strong lunar magnetic anomaly with a high-albedo region of the Descartes mountains. *Geophys. Res. Lett.* 30 (7), 1395. doi:[10.1029/2003GL016938](https://doi.org/10.1029/2003GL016938).
- Robinson, M.S., et al., 2010. Lunar reconnaissance orbiter camera (LROC) overview. *Space Sci. Rev.* 150, 81–124. doi:[10.007/s11214-010-9634-2](https://doi.org/10.007/s11214-010-9634-2).
- Robinson, M.S., Thangavelautham, J., Anderson, B.J., et al., 2015. Swirl – Unraveling the Enigma. *European Lunar Symposium*, Frascati, Italy.
- Sato, H., Robinson, M.S., Hapke, B., et al., 2014. Resolved Hapke parameter maps of the Moon. *J. Geophys. Res. Planets* 119 (8), 1775–1805. doi:[10.1002/2013JE004580](https://doi.org/10.1002/2013JE004580).
- Scholten, F., Oberst, J., Matz, K.-D., et al., 2012. GLD100: The near-global lunar 100 m raster DTM from LROC WAC stereo image data. *J. Geophys. Res.* 117, E00H17. doi:[10.1029/2011JE003926](https://doi.org/10.1029/2011JE003926).
- Schlitz, P.H., Srnka, L.J., 1980. Cometary collisions on the Moon and Mercury. *Nature* 284, 22–26.
- Starukhina, L.V., Shkuratov, Y.G., 2004. Swirls on the Moon and Mercury: Meteoroid swarm encounters as a formation mechanism. *Icarus* 167 (1), 136–147.
- Strom, R.G., Whitaker, E.A., 1969. An Unusual Far-Side Crater. *Apollo 10 Photography and Visual Observations*, NASA SP-232, pp. 20–24.
- Wells, E., Hapke, B., 1977. Lunar soil: Iron and titanium bands in the glass fraction. *Science* 195, 977–979.
- Whitaker, E.A., 1969. Sublimates. In: *Proceedings of Analysis of Apollo 8 Photography and Visual Observations*, NASA SP-201, pp. 34–35.
- Wieser, M., Barabash, S., Futaana, Y., et al., 2010. First observation of a mini-magnetosphere above a lunar magnetic anomaly using energetic neutral atoms. *Geophys. Res. Lett.* 37 (5), L05103. doi:[10.1029/2009GL041721](https://doi.org/10.1029/2009GL041721).
- Wilhelms, D.E., 1987. *The Geologic History of the Moon* (U. S. Geol. Surv. Prof. Paper 1348). United States Government Printing Office, Washington, DC.